Structures and cis-to-trans Photoisomerization of Hexafluoro-1,3-butadiene Radical Cation: Electron Spin Resonance and Computational Studies

Hong-Yan Xiao, Jun Cao, Ya-Jun Liu,* Wei-Hai Fang,* Hiroto Tachikawa, and Masaru Shiotani*

College of Chemistry, Beijing Normal University, Beijing, 100875, China, Graduate School of Engineering, Hokkaido University, Sapporo 060-8628, Japan, and Department of Applied Chemistry, Graduate School of Engineering, Hiroshima University, Higashi-Hiroshima, 739-8527, Japan

Received: January 26, 2007; In Final Form: April 18, 2007

The s-cis and s-trans isomer radical cations of hexafluoro-1,3-butadiene (*s-cis*-HFBD$^+$ and *s-trans*-HFBD$^+$) were generated by a γ-irradiated solid solution of the neutral HFBD molecule in solid matrix at 77 K and observed by means of electron spin resonance (ESR) and electronic spectroscopies. In comparing the experimental isotropic and anisotropic ^{19}F hyperfine splittings with the computational ones by the DFT B3LYP and MP2 methods, the generated *s-cis*-HFBD$^+$ and *s-trans*-HFBD$^+$ radical cations were confirmed to be $^2A_2$ and ^2B_g electronic ground states in C_{2v} and C_{2h} symmetries, respectively. The present spectroscopic study revealed that the relative abundance of *s-cis*-HFBD$^+$ to *s-trans*-HFBD$^+$ was 4.0 immediately after being formed by γ-irradiation, and subsequently most *s-cis*-HFBD$^+$ was isomerized to *s-trans*-HFBD$^+$ by visible-light illumination with 500−600 nm wavelength. The process of nonplanar HFBD ionizing to form stable planar *s-cis*- and *s-trans*-HFBD$^+$ and the reaction mechanism of the cis-to-trans photoisomerization were discussed by (MS-)CASPT2//CASSCF calculated vertical excitation energies (T_v) and torsional potential energy curves (TPECs) of HFBD and HFBD$^+$.

1. Introduction

Perfluorocarbons have remarkable chemical and physical properties such as chemical inertness, thermal stability, high hydrophobicity, low dielectric constant, and large electronegativity and have gained much attention and widespread applications.[1,2] The applications in modern technology such as etchants for semiconductor fabrication require a deeper understanding of the electronic structure, dynamics, and reactivity of the fluorocarbons.[3,4] A number of fluorinated hydrocarbon radical cations were subjected to electron spin resonance (ESR) studies during the past two decades,[5−9] but the detailed electronic structures and reactivities of perfluorocarbon radical ions have not yet been fully characterized.[10]

Along with the ESR studies of hydrocarbon radical cations, many of the ^{19}F hyperfine (hf) splittings (or couplings) have been well explained by quantum chemical theoretical calculations.[11−13] However, the presently targeted HFBD$^+$ is a tricky one. Neutral HFBD is of nonplanar structure with the carbon skeleton dihedral angle of 47.4° ± 2.4°,[14] while 1,3-butadiene has s-trans-planar structure.[15] This indicates that fluorine substitution has a significant effect on the geometric and electronic structures of 1,3-butadiene. However, when HFBD loses one electron to form HFBD$^+$, the structure changes back to the planar one.[16] In a previous paper one of the present authors[5] reported some preliminary experimental results showing two distinctly different ESR spectra of HFBD$^+$ generated and stabilized by γ-irradiation of a solid solution of HFBD in a halocarbon such as CF_2ClCF_2Cl (F-114) at 77 K. Based on the experimental spectrum analysis and the semiempirical INDO calculations, the ESR spectra were attributed to planar *s-cis*- and *s-trans*-HFBD$^+$ with π-type singly occupied molecular orbitals (SOMOs) a_2 (C_{2v}) and b_g (C_{2h}), respectively. Recently, Li et al.[13] computed the isotopic hf splittings of ^{19}F atoms of a series of fluorinated hydrocarbon radical cations, including HFBD$^+$, by means of the density functional theory[17,18] (DFT) Becke's three-parameter hybrid function[19] with the nonlocal correlation of Lee−Yang−Parr[20] (B3LYP) and the second-order Møller−Plesset perturbation theory[21,22] (MP2). However, they did not report the anisotropic ^{19}F hf splittings (*B* values), which are more important for discussing the geometric and electronic structures of the HFBD radical cations. Another unsolved problem is the theoretical explanation for the ESR experimentally observed phenomena: (1) the relative abundance of *s-trans*- and *s-cis*-HFBD$^+$ is 1:4 in the HFBD solution immediately after γ-irradiation at 77 K; (2) 80% *s-cis*-HFBD$^+$ cations turn to *s-trans*-HFBD$^+$ after illumination with visible light. The different relative abundance of *s-trans*- and *s-cis*-HFBD$^+$ subsequently affected the hf components in the experimental ESR spectra. The recent successful experimental and theoretical study[10] on a series of perfluoroalkene and perfluoroalkane radical anions inspired us to recalculate the electronic structures of HFBD$^+$.

In the present paper, the study on the HFBD radical cations was fully expanded both experimentally and theoretically. Experimentally, the ESR spectra were successfully simulated by using anisotropic ^{19}F hf splittings with a common principal axis system and the relative abundance of *s-trans*- and *s-cis*-HFBD$^+$ as variable parameters. This result strongly supports the previous assignment of the planar π-type structure of two HFBD$^+$ isomers. Furthermore, *s-cis*-HFBD$^+$ was observed to isomerize into *s-trans*-HFBD$^+$ by visible-light illumination with λ_{max} = 500−600 nm wavelength. The electronic absorption spectra were newly observed for both isomer radical cations. The result was found to be well consistent with the ESR results.

* Corresponding authors. E-mail: yajun.liu@bnu.edu.cn (Y.-J.L.); fangwh@bnu.edu.cn (W.-H.F.); mshiota@hiroshima-u.ac.jp (M.S.).

10.1021/jp070672c CCC: $37.00
Published on Web 05/25/2007

SCHEME 1

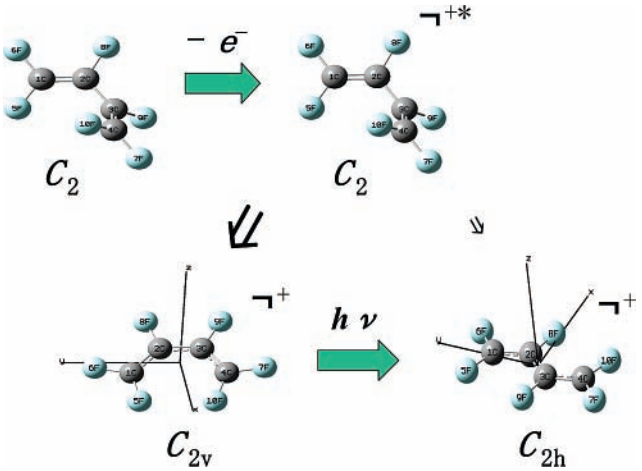

Theoretically, the DFT B3LYP and MP2 methods were employed to calculate the isotropic (a) and anisotropic (B_{ii}) ^{19}F hf coupling values of the two HFBD$^+$ isomers. The complete active space self-consistent field (CASSCF)[23,24] and multistate (MS) second-order perturbation (CASPT2)[25−27] methods were newly carried out to investigate the vertical excitation energies (T_v) values and torsional potential energy curves (TPECs) so as to discuss the cis-to-trans photoisomerization processes of HFBD$^+$. Furthermore, ionization of nonplanar HFBD by ionizing radiation and relaxation of the initial "hot" nonplanar HFBD$^+$ to the planar *s-cis*- and *s-trans*-HFBD$^+$ cations as outlined in Scheme 1 are discussed based on the present computations of the first ionization potential (I_p) of HFBD and the TPECs of both HFBD and HFBD$^+$.

2. Experimental Section

2.1. Experimental Method. Hexafluoro-1,3-butadiene (HFBD) was obtained from Peninsular Chemical Research (PCR, Inc.). The purity of the sample was examined by observing the Raman spectrum at 400 Torr using a JASCO R-88 spectrometer excited with an argon ion laser at 514.5 nm. The spectrum was identical to that previously reported by Wurrey et al.,[28] which was attributed to nonplanar *s-cis*-HFBD. Thus the HFBD used was concluded to be free of impurities. Halocarbons (>99%) such as F-114, $CF_2ClCFCl_2$ (F-113), and $CF_3CF(CF_3)CF_2CF_3$ (F-2MP) were commercially obtained from Tokyo Kasei Co. and used as matrixes without further purification. Solid solutions of ~0.5 mol % (mole percent) of the solute were degassed by several freeze−thaw cycles and then irradiated by γ-rays at 77 K. This is a well-known procedure to radiolytically generate the solute radical cations and subsequently stabilize them in the low-temperature solid matrix.[29] Photoillumination was made by using a 500 W xenon lamp equipped with an Ushio UI-501C lamp house and attached cutoff glass filters with cutoff wavelengths of 900, 660, 500, 350, and 250 nm. Hereinafter the lights passed through these filters are called IR900, VR600, VR500, UV350, and UV250 lights, respectively. The photobreaching experiments were done by light focused with a quartz lens attached to the lamp house for 5 min in the respective experiments at 77 K. The ESR and optical absorption spectra were measured at 77 K using FX-1X JEOL ESR and Hitachi U-3400 spectrometers, respectively.

2.2. Experimental Results and Discussion. *2.2.1. ESR Spectra.* Spectra A and B shown in Figure 1 were measured for a γ-irradiated solid solution of HFBD in F-114 before and after exposure to unfiltered light from a tungsten lamp at 77 K.

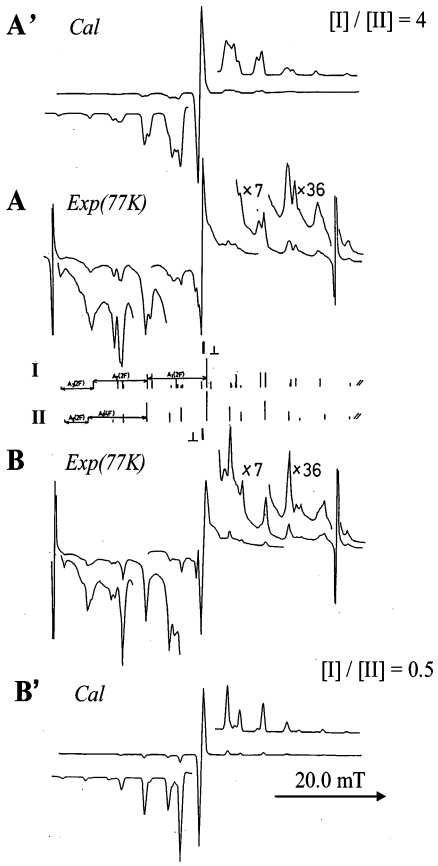

Figure 1. ESR spectra recorded at 77 K for a γ-irradiated 1 mol % hexafluoro-1,3-butadiene (HFBD) in CF_2ClCF_2Cl (F-114) matrix before (A) and after (B) exposure of the sample to unfiltered light from a tungsten lamp. A′ and B′ are the calculated spectra best fit to spectra A and B. The relative intensities of *s-cis*-HFBD$^+$ (I) to *s-trans*-HFBD$^+$ (II) are [I]/[II] = 4.0 and [I]/[II] = 0.5 for spectra A′ and B′, respectively. The ESR ^{19}F hf parameters used in the simulations are given in Table 1.

It is clearly seen that the ESR hf pattern becomes simpler by the light illumination. In the previous paper[5] we have reported that spectrum A consists of a superposition of ^{19}F hf lines due to two HFBD$^+$ isomers, *s-trans*-HFBD$^+$ and *s-cis*-HFBD$^+$, whereas spectrum B consists of only *s-trans*-HFBD$^+$. The parallel components of ^{19}F hf splittings are marked in the stick plots of Figure 1. In order to confirm the above assignment of the spectra and to estimate the relative abundance of the two radical cations, the ESR spectral simulation was carried out for both spectra, A and B. The ESR spectra of both the *s-trans*- and *s-cis*-HFBD$^+$ cations showed anisotropic line shape features and were successfully simulated based on the assumption of axially symmetric anisotropic ^{19}F hf structure with parallel ($A_{||}$) and perpendicular ($A_\perp$) splittings. Spectra A′ and B′ in Figure 1 are the simulated ones best fit to spectra A and B, respectively. The experimental ESR parameters used in the simulations are listed in Table 1. The present ESR simulations show that the $A_\perp$ values are close to zero, more exactly less than the Gaussian line width (0.6 mT) employed for both HFBD$^+$ isomers. The isotropic ^{19}F hf (a) splittings were derived from the anisotropic $A_{||}$ and $A_\perp$ splittings using the relation $a = (A_{||} + 2A_\perp)/3$. A broad underlying ESR signal, which is not assigned by the present simulations, can be seen in the experimental spectra, A and B, in Figure 1. The signal is attributable to the halocarbon matrix radicals, i.e., $CF_2ClCF_2Cl^-$ radical anion and/or its dissociation product, $CF_2ClCF_2^\bullet$ neutral radical, which were formed by the transfer of an electron generated by ionizing

TABLE 1: Calculated Isotropic (*a*) and Anisotropic (*A*) ^{19}F Hyperfine Coupling Constants (mT) of the *s-trans*- and *s-cis*-HFBD$^+$ Cations[a] in Comparison with the Experimental Ones

cation (state)	atom	computation method	A_{aa}	A_{bb}	A_{cc}	a
s-trans-HFBD$^+$ (^2B_g)	F6,7	B3LYP//B3LYP	11.41	−0.91	−1.32	3.05
		MP2//B3LYP	10.85	−0.10	−0.32	3.48
		MP2/6-31+G(d,p)//B3LYP/6-311+G(d,p)[b]				3.18
		INDO[c]				5.09
		exptl[c]	10.64	≈0	≈0	3.55
	F8,9	B3LYP//B3LYP	4.19	−0.44	−0.61	1.05
		MP2//B3LYP	4.84	0.43	−0.21	1.69
		MP2/6-31+G(d,p)//B3LYP/6-311+G(d,p)[b]				1.69
		INDO[c]				2.32
		exptl[c]	4.22	≈0	≈0	1.41
	F5,10	B3LYP//B3LYP	11.50	−0.90	−1.33	3.09
		MP2//B3LYP	10.91	−0.07	−0.28	3.52
		MP2/6-31+G(d,p)//B3LYP/6-311+G(d,p)[b]				3.10
		INDO[c]				5.01
		exptl[c]	10.64	≈0	≈0	3.55
s-cis-HFBD$^+$ ($^2A_2$)	F6,7	B3LYP//B3LYP	11.62	−0.93	−1.33	3.12
		MP2//B3LYP	11.01	−0.07	−0.34	3.54
		MP2/6-31+G(d,p)//B3LYP/6-311+G(d,p)[b]				3.22
		INDO[c]				5.45
		exptl[c]	10.62	≈0	≈0	3.54
	F8,9	B3LYP//B3LYP	5.57	−0.70	−0.71	1.39
		MP2//B3LYP	6.57	0.52	−0.06	2.34
		MP2/6-31+G(d,p)//B3LYP/6-311+G(d,p)[b]				2.26
		INDO[c]				2.34
		exptl[c]	6.07	≈0	≈0	2.02
	F5,10	B3LYP//B3LYP	10.68	−0.79	−1.28	2.87
		MP2//B3LYP	9.77	−0.15	−0.35	3.09
		MP2/6-31+G(d,p)//B3LYP/6-311+G(d,p)[b]				2.77
		INDO[c]				4.78
		exptl[c]	9.70	≈0	≈0	3.23

[a] For the atomic notations and the directions of *A*, see Figure 4. [b] Reference 13. [c] Reference 5.

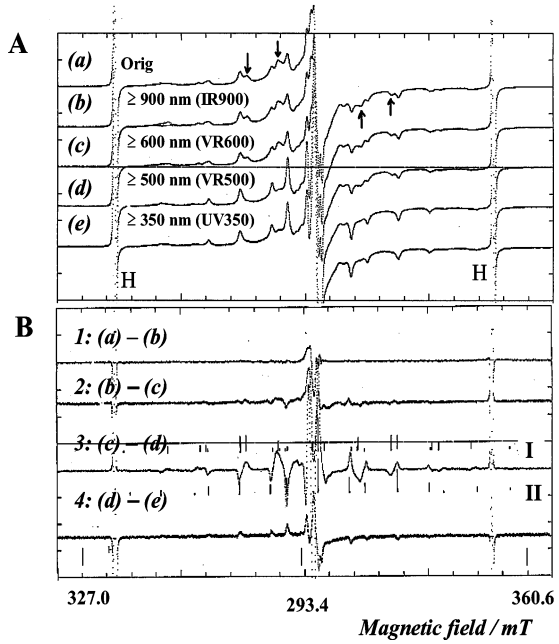

Figure 2. (A, upper) ESR spectra recorded for γ-irradiated 1 mol % hexafluoro-1,3-butadiene (HFBD) in CF_2ClCF_2Cl (F-114) before illumination (a) and after successive illumination by IR900 (b), VR600 (c), VR500 (d), and UV350 (e) lights. (B, lower) Difference spectra: 1 = (a) − (b), 2 = (b) − (c), 3 = (c) − (d), and 4 = (d) − (e). See details in the text.

radiation.[29a] Its radical intensity is almost equal to that of the sum of the solute *s-cis*- and *s-trans*-HFBD$^+$ radical cations.

Based on the ESR spectral simulations, the relative abundances of *s-cis*-HFBD$^+$ [I] to *s-trans*-HFBD$^+$ [II] were evaluated to be [I]/[II] = 4.0 and 0.5 for spectra A and B, respectively. The total ESR spectral intensity remained unchanged after the light illumination. These results suggest that *s-cis*-HFBD$^+$ was isomerized to *s-trans*-HFBD$^+$ by visible-light illumination. The obtained ESR parameters were characterized by the following three points. (1) They have the axial-symmetric ^{19}F ($I = 1/2$) hf splittings with a large anisotropy, $A_{||}$ ($=a + B_{||}$) > $A_{\perp}$ ($=a + B_{\perp}$), where a is isotropic hf splitting and $B_{||}$ and $B_{\perp}$ are parallel and perpendicular components of the anisotropic hf tensors where $B_{||} = B_{aa}$, $B_{\perp} = B_{bb} = B_{cc}$, and $B_{aa} + B_{bb} + B_{cc} = 0$. (2) The hf splittings observed for the three paired ^{19}F nuclei have a common principal direction. (3) No significant g-value shift from the free electron (g_e) was observed for the parallel component, i.e., $g_{||} \approx g_e$ (2.0023). The above results indicated that both the *s-trans*-HFBD$^+$ and *s-cis*-HFBD$^+$ radical cations take a planar π-type structure in the ground electronic states.

2.2.2. Photoisomerization from s-cis-HFBD$^+$ to s-trans-HFBD$^+$. In order to obtain information about wavelengths at which the photoisomerization from *s-cis*-HFBD$^+$ to *s-trans*-HFBD$^+$ takes place, the γ-irradiated sample was exposed to light from a xenon lamp with the cutoff filters. The ESR spectral changes are shown in Figure 2A(a)−(e): before illumination (a), and after illumination by IR900 (b), VR600 (c), VR500 (d), and UV350 (e) lights. The wavelength dependence can be clearly seen at the bands marked with arrows in Figure 2A. For example, the outermost bands among the marked ones were observed to be a doublet in spectrum a whose inner and outer lines are attributable to *s-cis*-HFBD$^+$ and *s-trans*-HFBD$^+$, respectively. By VR500 light illumination the inner line decreased sharply in intensity with concomitant increase of the outer line as described in spectra c and d. As the difference spectra in Figure 2B show, when the signals decrease (increase) by illumination, the difference spectrum appears with plus (minus) phases in the lower field side, but with minus (plus)

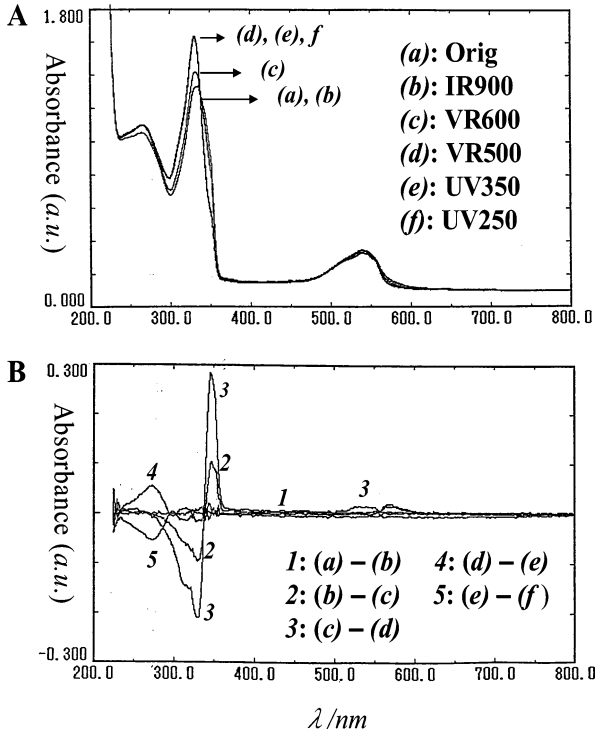

Figure 3. (A, upper) Optical absorption spectra of γ-irradiated 1 mol % hexafluoro-1,3-butadiene (HFBD) in perfluoro-2-methylpentane (F-2MP) matrix before illumination (a) and after successive illumination by IR900 (b), VR600(c), VR500 (d), UV350 (e), and UV250 (f) lights. (B, lower) Difference spectra: 1 = (a) − (b), 2 = (b) − (c), 3 = (c) − (d), and 4 = (d) − (e). See details in the text.

phases in the higher field side. The largest spectral change was observed in the difference spectrum 3 = (c) − (d). This clearly shows that the concomitant of *s-trans*-HFBD$^+$ is increasing with *s-cis*-HFBD$^+$ decaying by VR500 light illumination. Furthermore, UV350 light illumination resulted in a slight decrease of *s-trans*-HFBD$^+$ as depicted by the difference spectrum 4 = (d) − (e). During photoillumination with wavelength $\lambda > 500$ nm, the radical concentration remained unchanged. In fact, the double integrations of first derivative spectra a−d in Figure 2A are constant within 1% error. Thus we confirmed in the present experiments that *s-cis*-HFBD$^+$ was most efficiently isomerized to *s-trans*-HFBD$^+$ by light illumination with wavelengths of $600 > \lambda > 500$ nm. In addition, we observed the following results in the present ESR experiments. First, the reverse isomerization from *s-trans*-HFBD$^+$ to *s-cis*-HFBD$^+$ was not observed. Second, the same experimental results were repeated but with lower ESR spectral resolution by using F-113 as matrix instead of F-114. Finally, upon warming the sample from 77 to 105 K, the signals of *s-cis*-HFBD$^+$ decayed, whereas those of *s-trans*-HFBD$^+$ remained almost unchanged. The result suggests that *s-cis*-HFBD$^+$ is thermally less stable than *s-trans*-HFBD$^+$.

2.2.3. Electronic Spectra of HFBD$^+$. Figure 3A shows the electronic spectra of a γ-irradiated 1 mol % HFBD in F-2MP matrix before illumination (a) and after successive illumination by IR900 (b), VR600 (c), VR500 (d), UV350 (e), and UV250 (f) lights. F-2MP has no absorption bands in the wavelength range above 300 nm wavelength. This is the reason F-2MP was chosen to be the matrix in the present study of HFBD$^+$ electronic spectra. Above 300 nm, the original spectrum ((a) in Figure 3A) consists of a weak broad absorption band and a strong sharp one at 500−600 and 300−350 nm, respectively. The observation of the absorption band at 500−600 nm is consistent with the ESR experimental results discussed above, which further confirms that the cis-to-trans photoisomerization occurred by the visible-light illumination of $\lambda = 500-600$ nm.

Figure 3B shows the difference in the electronic spectra, where the positive and negative side peaks correspond to decaying and increasing in the absorption bands by light illumination. According to Figure 3B, the largest two spectral changes were observed for the light illuminating with VR500, in the bands of 500−600 and 300−350 nm. The former change is much smaller than the latter, suggesting smaller oscillator strength (f) in the former band. The positive side peak at $\lambda_{max} = \sim 350$ nm corresponds to the decaying, whereas the negative side peak at $\lambda_{max} = \sim 330$ nm corresponds to the increasing. The decaying is concomitantly followed by the increasing, which is in a situation quite similar to the ESR observations discussed in section 2.2.2. Thus the absorption bands with ∼350 and ∼330 nm λ_{max} could come from *s-cis*-HFBD$^+$ and *s-trans*-HFBD$^+$, respectively.

The shorter wavelength illumination ($500 > \lambda > 350$ nm) was performed on a radical cation sample which had been already illuminated by the longer wavelength light at $600 > \lambda > 500$ nm, i.e., on an "old" sample. Thus, once the photoisomerization from *s-cis*-HFBD$^+$ to *s-trans*-HFBD$^+$ occurs at the longer wavelength, there are no *s-cis*-HFBD$^+$ radical cations left to isomerize at the shorter wavelength. This is the reason no photoisomerization was observed for the shorter wavelength illumination although the *s-cis*-HFBD$^+$ radical cation has an absorption band at ∼350 nm. The electronic spectra of HFBD$^+$ will be further discussed by theoretical calculations in section 3.2.3.

3. Computational Section

3.1. Computational Details. The geometric optimizations and frequency analyses of HFBD, *s-trans*-HFBD$^+$,and *s-cis*-HFBD$^+$ were carried out by B3LYP and CASSCF methods. The isotropic a and anisotropic B_{ii} ($i = a, b, c$) hf splittings on the ^{19}F atoms (with nuclear spin $I = 1/2$) of *s-trans*- and *s-cis*-HFBD$^+$ were calculated by B3LYP//B3LYP and MP2//B3LYP methods. The (MS-)CASPT2//CASSCF method was employed to calculate the I_p value of HFBD and the T_v values and TPECs of HFBD, *s-trans*-HFBD$^+$, and *s-cis*-HFBD$^+$. All the B3LYP and MP2 calculations employed AUG-cc-pVDZ basis set[30,31] to C and F atoms and were performed using the Gaussian 03 program package.[32] Those CASSCF and (MS-)CASPT2 calculations were performed using MOLCAS 6.2 quantum chemistry software,[33,34] in conjunction with the relativistic basis sets of the atomic natural orbital type, ANO-RCC,[35−37] in which the C and F bases were contracted to 3s2p1d. The selection of active electrons and spaces is 12-in-10 for the HFBD molecule and 11-in-10 for the HFBD$^+$ cations.

3.2. Computational Results and Discussion. *3.2.1. Geometric Structures.* Geometric optimizations of HFBD were carried out by the B3LYP/AUG-cc-pVDZ and CASSCF/ANO-RCC methods. The optimized geometric parameters are compared with the previously calculated[38] and experimental results[14] in Table 2. The related atom notations are given in Figure 4. Both the B3LYP and CASSCF frequency analyses of HFBD indicated that the optimized geometries are at the total energy minima and the calculated vibrational frequencies are in agreement with the corresponding experimental values;[28] see the Supporting Information. The electron diffraction study revealed that neutral HFBD is of nonplanar structure with 47.4° ± 2.4° dihedral angle C1−C2−C3−C4 (β).[14] The previous calculations[38−40] also predicted nonplanar HFBD with β from 45.0° to 64.0° depending on different computational method

TABLE 2: Calculated Equilibrium Geometric Structures of Neutral HFBD, *s-trans*-HFBD$^+$, and *s-cis*-HFBD$^+$ at the CASSCF/ANO-RCC and B3LYP/AUG-cc-pVDZ Levels,[a,b] Together with the Crossing Point of the PECS of *s-trans*- and *s-cis*-HFBD$^+$ Optimized at the CASSCF/ANO-RCC Level

	HFBD				*s-trans*-HFBD$^+$			*s-cis*-HFBD$^+$			
geom params	CASSCF	B3LYP	previous[c]	exptl[d]	CASSCF	B3LYP	previous[e]	CASSCF	B3LYP	previous[e]	crossing point
R(C1−C2)	1.340	1.337	1.329	1.336 ± 0.018	1.402	1.399	1.396	1.401	1.397	1.394	1.402
R(C2−C3)	1.452	1.451	1.447	1.488 ± 0.018	1.390	1.411	1.408	1.401	1.421	1.418	1.424
R(C1−F5)	1.294	1.323	1.312	1.323 ± 0.006	1.250	1.284	1.277	1.253	1.287	1.281	1.252
R(C1−F6)	1.288	1.319	1.316	1.323 ± 0.006	1.248	1.282	1.275	1.248	1.282	1.274	1.248
R(C2−F8)	1.322	1.359	1.353	1.323 ± 0.006	1.288	1.322	1.316	1.286	1.319	1.313	1.295
−(C2−C3−C4)	125.1	125.8	125.8	125.8 ± 0.6	125.1	125.0	124.7	130.2	130.4	130.5	123.0
−(C2−C3−F9)	116.2	116.3	116.4		119.1	119.0	119.2	115.4	114.9	114.8	116.9
−(C3−C4−F7)	124.5	124.0	123.9	124.5 ± 0.6	120.9	120.9	120.8	120.5	120.5	120.5	121.4
−(C3−C4−F10)	123.2	124.1	124.1		123.2	123.7	123.6	124.0	124.6	124.4	123.0
dihedral angle β	56.4	57.7	58.4	47.4 ± 2.4	180.0	180.0	180.0	0.0	0.0	0.0	90.0

[a] For the atomic notations, see Figure 4. [b] Bond lengths in Å (angstroms), angles in degrees. [c] B3LYP/6-311+G(2d) calculation in ref 38. [d] Reference 14. [e] B3LYP/6-311+G(d,p) calculation in ref 13.

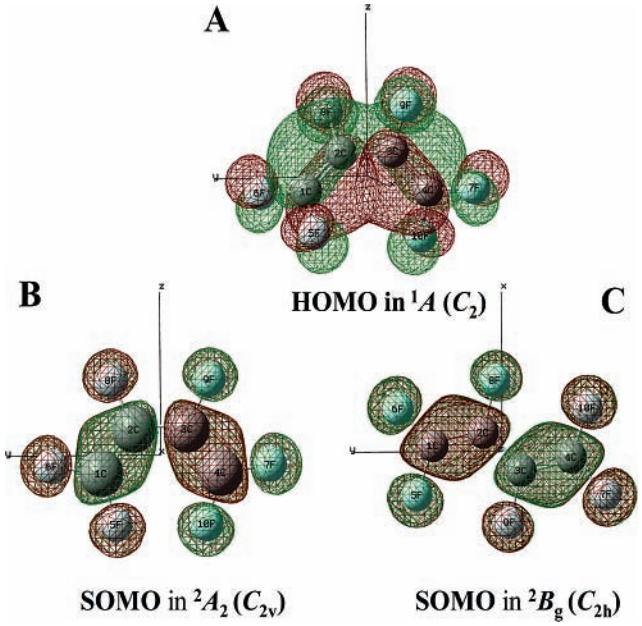

Figure 4. B3LYP/AUG-cc-pVDZ optimized structures together with the *x*,*y*,*z*-coordinate system and the HOMO or SOMO plots of (A) HFBD ^{1}A (C_2), (B) *s-cis*-HFBD$^+$ ^{2}A (C_{2v}), and (C) *s-trans*-HFBD$^+$ ^{2}B$_g$ (C_{2h}) ground states. The anisotropic ^{19}F hf splittings of $A_{||}$ and $A_{\perp}$ are parallel and perpendicular to the *x*-axis for *s-cis*-HFBD$^+$, respectively, whereas they are parallel and perpendicular to the *z*-axis for *s-trans*-HFBD$^+$.

used. The present B3LYP/AUG-cc-pVDZ (CASSCF/ANO-RCC) optimization resulted in $\beta = 57.7°$ (56.4°), which is (unexpectedly) by 8−12° larger than the experimental values.[14] Karpfen et al.[38] reported $\beta = 58.4°$ for the optimized structure at B3LYP/6-311+G(2d) level. These large deviations between the experimental and computed β values could originate from the assumptions used in analyzing the experimental data observed in the gas-phase electron diffraction study.[14] The presently B3LYP and CASSCF optimized C=C, C−C, and C−F bond lengths and all the bond angles are in good agreement with the corresponding experimental values[14] except for the β angle; see Table 2.

In contrast to the neutral HFBD molecule, the radical cations are of planar structures. The B3LYP/AUG-cc-pVDZ and CASSCF/ANO-RCC optimized geometries of *s-trans*-HFBD$^+$ (C_{2h} symmetry) and *s-cis*-HFBD$^+$ (C_{2v} symmetry) are similar to the previously B3LYP/6-311+G(d) optimized ones,[13] respectively, as shown in Table 2. The related atom notations are given in Figure 4. The B3LYP and CASSCF frequency analyses (at the same computational level) indicated that the presently optimized ^{2}B$_g$ (C_{2h}) state of *s-trans*-HFBD$^+$ and the ^{2}A$_2$ (C_{2v}) state of *s-cis*-HFBD$^+$ are the ground electronic states. Both the B3LYP and CASSCF calculated frequencies of the *s-trans*-HFBD$^+$ and *s-cis*-HFBD$^+$ cations are tabulated in the Supporting Information together with those of neutral HFBD.

As shown in Table 2, the bond length of C1−C2 (C3−C4) is elongated by about 0.06 Å when the original neutral one catches a hole to form the radical cations *s-trans*-HFBD$^+$ and *s-cis*-HFBD$^+$ at both the B3LYP/AUG-cc-pVDZ and CASSCF/ANO computational levels. The bond elongation is due to removal of one electron from the π-type bonding molecular orbital. Certainly, the most important change from HFBD to HFBD$^+$ is the dihedral angle β, which is forced to change from the original value of ∼57° to 0° and 180°.

3.2.2. Isotropic and Anisotropic ^{19}F hf Splittings of s-cis-HFBD$^+$ and s-trans-HFBD$^+$. Figure 4 shows the B3LYP/AUG-cc-pVDZ calculated plots of the SOMOs: b$_g$ orbital for *s-trans*-HFBD$^+$ (C_{2h}) and a$_2$ orbital for *s-cis*-HFBD$^+$ (C_{2v}). Both b$_g$ and a$_2$ orbitals are composed of antibonding π-type interactions for all C− F bonds.

In previous studies, the isotropic ^{19}F hf splittings were computed for both HFBD$^+$ isomers by INDO,[5] B3LYP, and MP2[13] methods. In the present study we still used the B3LYP and MP2 methods, but with bigger basis sets, and computed both the isotropic and anisotropic hf splittings of the ^{19}F atoms. The results are summarized and compared with the previously calculated[13] and the experimental ones in Table 1.

As shown in Table 1, the MP2//B3LYP predicted isotropic hf splittings of F6,7, F8,9, and F5,10 for *s-trans*-HFBD$^+$ and *s-cis*-HFBD$^+$ are in excellent agreement with the respective experimental ones, and better than the MP2/6-31+G(d,p)//B3LYP/6-311+G(d,p)[13] predicted ones, respectively. The B3LYP//B3LYP computations resulted in the isotropic ^{19}F hf splittings of the two HFBD$^+$ cations which are smaller by about 0.4−0.6 mT than the respective experimental values; the agreements are slightly worse than the MP2//B3LYP computations.

The anisotropic A_{aa}, A_{bb}, and A_{cc} ^{19}F hf splittings were computed by the B3LYP//B3LYP (MP2//B3LYP) method, and the results are summarized in Table 1 together with the experimental ones.[5] The computed A_{bb} and A_{cc} splittings coincide with each other within 0.41 mT (the maximum difference for F6,7 computed by B3LYP//B3LYP). The difference is smaller than the experimental line width (0.6 mT). This ascertains the validity of the assumption of axially symmetric anisotropic ^{19}F hf splittings, $A_{aa} \approx A_{||}$ and $A_{bb} \approx A_{cc} \approx A_{\perp}$, used in the ESR

TABLE 3: Comparison of Calculated and Experimental Vertical Excitation Energies T_v (in eV) and Oscillator Strengths f of the First Five Excited States of HFBD

MS-CASPT2					CIS[a]				
state[c]	T_v	f	character[d]		state[c]	T_v	f	character[d]	exptl[b]
S_1-A	6.2	0.0014	$\pi\pi^*$	HOMO − 1 → LUMO HOMO → LUMO + 1					
S_2-B	6.5	0.3054	$\pi\pi^*$	HOMO → LUMO	S_1	7.5	0.47	$\pi\pi^*$	6.3
S_3-A	7.5	0.2647	$\pi\pi^*$	HOMO − 1 → LUMO HOMO → LUMO + 1	S_6	9.6	0.37	$\pi\pi^*$	7.6
S_4-B	7.8	0.2167	$\pi\pi^*$	HOMO − 1 → LUMO + 1					
S_5-A	8.6	0.0411	$\pi\pi^*$	HOMO → LUMO + 2 HOMO → LUMO					

[a] Reference 41. [b] Reference 16. [c] Excited state to which electron transitions take place from the ground S_0 state. [d] Character of electronic transition.

TABLE 4: MS-CASPT2//CASSCF Calculated T_v (in eV) and f Values of the First Four Excited States of *s-trans*-HFBD$^+$ and *s-cis*-HFBD$^+$, Compared with the Available Experimental Values (in Parentheses)

s-trans-HFBD$^+$			*s-cis*-HFBD$^+$		
state	T_v	f	state	T_v	f
1-^2B_g	0.0		1-$^2A_2$	0.0	
1-^2A_u	2.6 (2.1−2.5)[a]	0.0373	1-$^2B_1$	2.5 (2.1−2.5)[a]	0.0335
2-^2A_u	4.1 (∼3.8)[a]	0.5524	2-$^2B_1$	3.9 (∼3.5)[a]	0.3934
1-^2A_g	5.5	0.0000	1-$^2A_1$	5.7	0.0000
2-^2B_g	6.5	0.0000	2-$^2A_2$	6.3	0.0060

[a] Present experiments.

spectral simulations. Furthermore, the largest A_{bb} or A_{cc} values predicted by the present B3LYP//B3LYP (MP2//B3LYP) are −1.33 mT (0.43 mT) for *s-trans*-HFBD$^+$, and −1.33 mT (0.52 mT) for *s-cis*-HFBD$^+$. The hf splittings of A_{bb} and A_{cc} computed by MP2//B3LYP method are less than the line width (0.6 mT) and in better agreement with the experimental values ($A_\perp$) than those by B3LYP//B3LYP. Consistent with the experimental prediction, the directions of A_{bb} and A_{cc} tensor components are in the molecular plane, i.e., the $x-y$ plane for *s-trans*-HFBD$^+$ and the $y-z$ plane for *s-cis*-HFBD$^+$; see Figure 4.

All the directions of A_{aa} tensor components are parallel to the z-axis for *s-trans*-HFBD$^+$ and to the x-axis for *s-cis*-HFBD, i.e., perpendicular to the $x-y$ plane for *s-trans*-HFBD$^+$ and the $y-z$ plane for *s-cis*-HFBD$^+$, respectively, consistent with those predicted from the experimental data (see Figure 4). Both the B3LYP and MP2 calculated A_{aa} values of *s-trans*-HFBD$^+$ and *s-cis*-HFBD$^+$ are close to the corresponding experimental values. The MP2//B3LYP calculations are slightly better than the B3LYP//B3LYP.

The excellent agreement of isotropic and anisotropic ^{19}F hf splittings between the present calculations and the experimental values ensures the assignment that spectrum A in Figure 1 was predominated by the *s-cis*-HFBD$^+$ cation, while spectrum B was predominated by the *s-trans*-HFBD$^+$. By comparison with the previously calculated and experimental results, the presently employed MP2//B3LYP and B3LYP//B3LYP computational methods are reliable for predicating ^{19}F hf splittings of organofluorine radicals.

3.2.3. Vertical Excitation Energy (T_v) and Oscillator Strength (f) of HFBD and HFBD$^+$. The electronic absorption spectrum of HFBD vapor exhibits two broad $\pi\pi^*$ transitions at 6.3 and 7.6 eV with similar intensities,[16] respectively. The MS-CASPT2//CASSCF calculated T_v values of the first five excited states, S_1-A, S_2-B, S_3-A, S_4-B, and S_5-A, to be 6.2, 6.5, 7.5, 7.8, and 8.6 eV with f values of 0.0014, 0.3054, 0.2647, 0.2167, and 0.0411, respectively. Based on the T_v and f values, both S_1-A and S_2-B should be responsible for the experimentally detected first transition of 6.3 eV,[16] and both S_3-A and S_4-B should be responsible for the second one of 7.6 eV.[16] Each line consists of the unresolved two transitions. This could be the reason that both the observed first and second lines are broad.[16] The present MS-CASPT2//CASSCF calculated results are much better than the previous CIS calculated 7.5 and 9.6 eV,[41] respectively, as shown in Table 3. Also, the CASPT2//CASSCF calculated 10.3 eV I_p agrees well with the experimental value of 10.4 eV.[16]

The success of MS-CASPT2//CASSCF calculations interpreting the HFBD electronic spectrum encouraged us to continue the same computations for the HFBD$^+$ radical cations. These calculations are necessary supports to the later discussion of cis-to-trans photoisomerization. The T_v and f values of the first four excited states of *s-cis*-HFBD$^+$ and *s-trans*-HFBD$^+$ computed at the MS-CASPT2//CASSCF level are summarized in Table 4. The calculated first two excited states of *s-trans*-HFBD$^+$ are 1-^2A_u and 2-^2A_u with T_v (f) values of 2.6 (0.0373) and 4.1 eV (0.5524), respectively. For *s-cis*-HFBD$^+$, the calculated first two excited states are 1-$^2B_1$ and 2-$^2B_1$ with 2.5 (0.0335) and 3.9 eV (0.3934) T_v (f) values. Comparing the above T_v values with the present electronic spectra and basing on the rough assignments in section 2.2.3, the experimentally observed first electron absorption band at $\lambda = 500-600$ nm (2.1−2.5 eV) is identified with the first excited states of both *s-cis*- and *s-trans*-HFBD$^+$ radical cations, and the second absorption bands with ∼350 (∼3.5) and ∼330 nm (∼3.8 eV) λ_{max} are identified with the second excited states of *s-cis*-HFBD$^+$ and *s-trans*-HFBD$^+$, respectively, as shown in Table 4. The MS-CASPT2//CASSCF calculated f value of the first excited state is much smaller than that of the second excited state for both *s-cis*-HFBD$^+$ and *s-trans*-HFBD$^+$. This is consistent with the experimental observation that the first absorption band is much weaker than the second one; see section 2.2.3.

3.2.4. Torsional Potential Energy Curves (TPECs) of HFBD and HFBD$^+$. The calculations of the TPECs are prepared for the later discussions of sections 3.2.5 and 3.2.6. We used the CASSCF method to optimize all other structural parameters of the HFBD ground state for a set of fixed dihedral angles in the range 0−180° in steps of 20°, and the energy was evaluated for these geometries by the CASPT2 method. The TPEC of the HFBD ground state is shown in the lower half of Figure 5. The

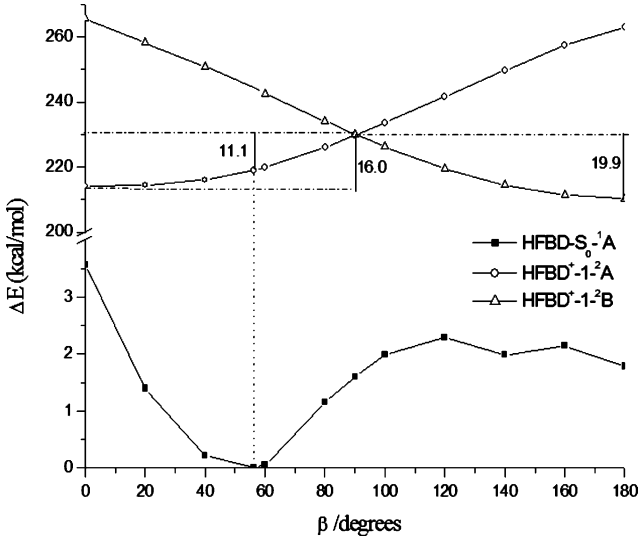

Figure 5. CASPT2//CASSCF calculated ground-state torsional potential energy curve (TPEC) of HFBD and TPECs of the first two states of $HFBD^+$ in C_2 symmetry.

CASPT2//CASSCF calculated TPEC of S_0-A further indicated that the nonplanar HFBD ($\beta = 56.4°$ by the CASSCF optimization) is the most stable, which is 1.8 and 3.6 kcal/mol more stable in energy than *s-trans*-HFBD and *s-cis*-HFBD, respectively. The previous HF calculated corresponding values are 1.8 and 5.7 kcal/mol.[39]

As seen in Table 2, the $HFBD^+$ radical cation has two energy minima at $\beta = 0°$ and 180°, which correspond to the s-cis-planar (C_{2v}) and s-trans-planar (C_{2h}) structures, respectively. Similar to the calculations of the HFBD TPEC, the TPECs of the first ^{2}A and first ^{2}B states of $HFBD^+$ in C_2 symmetry were calculated by the CASPT2//CASSCF method; see the upper half of Figure 5. At $\beta = 0°$, the C_2 symmetry turns to C_{2v}; simultaneously, the ^{2}A and ^{2}B states turn to the ground state 1-$^2A_2$ and first excited state 1-$^2B_1$ of *s-cis*-$HFBD^+$, respectively. At $\beta = 180°$, the C_2 symmetry turns to C_{2h}; accordingly, the ^{2}B and ^{2}A states turn to the ground state 1-^2B_g and first excited state 1-^2A_u of *s-trans*-$HFBD^+$. See both Figure 5 and Table 2. The ground state ^2B_g of *s-trans*-$HFBD^+$ is more stable by 3.9 kcal/mol than the ground state $^2A_2$ of *s-cis*-$HFBD^+$ based on CASPT2//CASSCF calculations and 3.2 kcal/mol by the B3LYP/AUG-cc-pVDZ computations. B3LYP/6-311+G(d)[13] and INDO[5] predicted this value to be 3.6 and 5.0 kcal/mol, respectively.

The present calculations support the ESR experimental results showing that the $HFBD^+$ possibly takes both the planar s-trans and s-cis structures and the former structure is thermally more stable than the latter one. As depicted in Figure 5, the TPECs of the 1-^{2}A and 1-^{2}B states in C_2 symmetry cross each other at $\beta = 90°$. The potential barrier from the planar s-cis to the planar s-trans is 16.0 kcal/mol, whereas it is 19.9 kcal/mol from s-trans to s-cis by CASPT2//CASSCF calculations. The CASSCF optimized geometry of the crossing point at $\beta = 90°$ is also tabulated in Table 2.

3.2.5. Ionization of HFBD and Relaxation of Non-Planar "Hot HFBD$^+$". The present ESR study revealed that the relative abundance of planar *s-cis*-$HFBD^+$ to planar *s-trans*-$HFBD^+$ is 4.0 immediately after being formed by γ-irradiation in the low-temperature solid matrix. As mentioned in section 2.1, the purity of HFBD used in the present experiments was examined by Raman spectroscopy. Based on the experimental spectrum, which is identical to the previously reported one,[28] the HFBD used was attributed to the nonplanar s-cis-type rotamer and free of impurities including s-trans-type rotamer. This leads us to conclude that the HFBD used contains only the s-cis-type rotamer and rules out a possibility of a ground-state distribution of s-cis-type to s-trans-type rotamers leading to respective s-cis-type and s-trans-type cation radicals. It is of interest to discuss the reasons the *s-cis*-$HFBD^+$ cation predominates over the *s-trans*-$HFBD^+$ cation even though the former cation is energetically less stable than the latter one. Here we discuss this problem in terms of ionization of "nonplanar HFBD" and successive relaxation of the initially formed "hot" cation to the planar *s-cis*- and *s-trans*-$HFBD^+$ cations; cf. Scheme 1.

The CASPT2//CASSCF calculated 10.3 eV I_p value of HFBD is in excellent agreement with the experimental value of 10.4 eV.[16] Neutral HFBD has a nonplanar "cisoid" geometric structure with a 56.4° dihedral angle β by CASSCF optimization. One electron can be easily transferred from the nonplanar HFBD molecule to the positively charged halocarbon matrix molecule to form $HFBD^+$ since the matrixes F-113 and F-114 have about 2 eV higher I_p values than HFBD, which are 11.98 and 12.66 eV,[29a] respectively. The initially formed $HFBD^+$ may keep its original nonplanar structure, which is in a vibrationally excited state (hot cation). Then, the nonplanar $HFBD^+$ will relax to energetically more favorable structures via internal rotation about the C2−C3 bond. As depicted in Figure 5, the CASPT2//CASSCF calculations predicted that this rotation (or relaxation) to *s-cis*-$HFBD^+$ along the 1-^{2}A state is exothermic by 3.9 kcal/mol and energetically favorable. On the other hand, the relaxation to *s-trans*-$HFBD^+$ has to pass the crossing point of the TPECs of ^{2}A and ^{2}B states; see Figure 5. It needs to overcome an 11.1 kcal/mol potential barrier and is an energetically more difficult process. However, the *s-trans*-$HFBD^+$ cation is more stable by 3.9 kcal/mol than the *s-cis*-$HFBD^+$ cation by the CASPT2//CASSCF calculations. Moreover, when one electron is transferred from the nonplanar HFBD to the irradiated matrixes to form $HFBD^+$, the 2 eV (46.1 kcal/mol) excess energy to the irradiated halocarbon matrixes to form $HFBD^+$ easily overcomes the 11.1 kcal/mol potential barrier to form more stable *s-trans*-$HFBD^+$. Thus there are two competitive channels: the first one to *s-cis*-$HFBD^+$ is more favorable for exothermicity, while the second one to *s-trans*-$HFBD^+$ is also possible to form a more stable product. It is the reason that spectrum A in Figure 1 consists of two ESR hf components due to the presence of both *s-cis*- and *s-trans*-$HFBD^+$, and the former is dominant. In the end we note that the following reactions cannot be completely ruled out as an alternative possibility: the oxidative electron transfer from the s-cis rotamer of HFBD (i.e., at 60°) produces the first excited electronic state of the cation radical (i.e., 1-^{2}B state in Figure 5), which relaxes to the conical intersection and produces the experimentally observed distribution of s-cis/s-trans-type rotamers of $HFBD^+$ at 77 K.

3.2.6. cis-to-trans Photoisomerization of HFBD$^+$. When the γ-irradiated sample solution at 77 K was illuminated by 500−600 nm visible light, the experiment observed that 80% *s-cis*-$HFBD^+$ turned to *s-trans*-$HFBD^+$. According to Table 4, the T_v of the first excited state 1-$^2B_1$ of *s-cis*-$HFBD^+$ is 2.5 eV (wavelength $\lambda = 495$ nm). This value corresponds well to the experimental results showing that the cis-to-trans isomerization occurs by 500−600 nm light illumination. It suggests that, once the ground state 1-$^2A_2$ of *s-cis*-$HFBD^+$ is excited by light to form the first excited state 1-$^2B_1$, the 1-$^2B_1$ state easily slides down to the ground state of *s-trans*-$HFBD^+$, 1-^2B_g, via the crossing point with 90° β value; see Figure 5. On the other hand, the 2.6 eV T_v of the first excited state 1-^2A_u of *s-trans*-

$HFBD^+$ is almost the same as that in *s-cis*-$HFBD^+$. However, the experimental results showed that no trans-to-cis isomerization was observed. The most important reason is that the ground state 1-^2B_g of *s-trans*-$HFBD^+$ is 3.9 kcal/mol more stable than the ground state 1-$^2A_2$ of *s-cis*-$HFBD^+$ as mentioned above. The potential barrier from s-cis to s-trans is 16.0 kcal/mol, whereas it is 19.9 kcal/mol from s-trans to s-cis by CASPT2//CASSCF calculations.

4. Conclusion

The structure and reactions of *s-cis*-$HFBD^+$ and *s-trans*-$HFBD^+$, which were radiolytically generated in low-temperature solid matrix, were studied by ESR and electronic spectroscopies and computations. The experimental isotropic and anisotropic ^{19}F hf splittings of both isomer radical cations were good compared with the computational ones by the DFT B3LYP and MP2 methods. The *s-cis*-$HFBD^+$ and *s-trans*-$HFBD^+$ cations were concluded to take $^2A_2$ (C_{2v} symmetry) and ^2B_g (C_{2h} symmetry) electronic ground states, respectively.

The present ESR study revealed that the *s-cis*-$HFBD^+$ cation predominates over the *s-trans*-$HFBD^+$ cation (with 4:1 abundance ratio) immediately after being formed in the matrix. This was well explained by the CASPT2//CASSCF calculated I_p of HFBD and the TPECs of HFBD and $HFBD^+$. Neutral HFBD is of nonplanar structure with 56.4° β value by CASSCF optimization. The hot $HFBD^+$ cation formed by HFBD catching one hole from the irradiated matrix molecule has about 2 eV (46.1 kcal/mol) excess energy, since the matrixes F-113 and F-114 have about 2 eV higher I_p than HFBD. The hot $HFBD^+$ cations have two competitive channels to relax to more stable planar $HFBD^+$. The first one to *s-cis*-$HFBD^+$ is more favorable for 4.9 kcal/mol exothermicity, while the second one to *s-trans*-$HFBD^+$ also has possibility since *s-trans*-$HFBD^+$ is 3.9 kcal/mol lower in energy than *s-cis*-$HFBD^+$, and the about 46.1 kcal/mol excess energy of the hot $HFBD^+$ cation can easily pass the crossing point of the TPECs of ^2A and ^2B states (see Figure 5) which has 11.1 kcal/mol higher energy than the hot $HFBD^+$ cation.

The present spectroscopic study revealed that the *s-cis*-$HFBD^+$ cation is isomerized to the *s-trans*-$HFBD^+$ by visible-light illumination with $500 < \lambda < 600$ nm at 77 K. The cis-to-trans photoisomerization was explained via the (MS-)CASPT2//CASSCF calculated T_v, and 1-^2A and 1-^2B TPECs of $HFBD^+$. The 2.5 eV (495 nm) T_v of the first excited state 1-$^2B_1$ of *s-cis*-$HFBD^+$ corresponds to the experimental result that the cis-to-trans isomerization occurs by 500−600 nm light illumination. Once the ground state 1-$^2A_2$ of *s-cis*-$HFBD^+$ is excited by the light to form the first excited state 1-$^2B_1$, the 1-$^2B_1$ state easily slides down to the ground state of *s-trans*-$HFBD^+$, 1-^2B_g, via the TPEC crossing point of the 1-^2A and 1-^2B states of $HFBD^+$. The potential barrier from cis to trans is 16.0 kcal/mol, whereas it is 19.9 kcal/mol from trans to cis. Thus, the cis-to-trans isomerization is much more favorable.

Acknowledgment. We appreciate the financial support of this work that was provided by the National Natural Science Foundation Committee of China (Nos. 20673012 and 20472011) and the Major State Basic Research Development Programs (Nos. 2004CB719903 and 2002CB613406). We are also indebted to Mr. Jirou Kawazoe and Prof. Takahisa Ichikawa for their help in recording ESR and optical spectra.

Supporting Information Available: Comparison of the calculated and experimental harmonic vibrational frequencies of HFBD, *s-trans*-$HFBD^+$, and *s-cis*-$HFBD^+$. This material is available free of charge via the Internet at http://pubs.acs.org.

References and Notes

(1) Green, S. W.; Slinn, D. S. L.; Simpson, R. N. F.; Woytek, A. J. In *Organofluorine Chemistry, Principles and Commercial Applications*; Banks, R. E., Smart, B. E., Tatlow, J. C., Eds.; Plenum: New York, 1994; p 89.

(2) Barthe-Rosa, L. P.; Gladysz, J. A. *Coord. Chem. Rev.* **1999**, *190*, 587.

(3) (a) Takahashi, K.; Ithoh, A.; Nakamura, T.; Tachibana, K. *Thin Solid Films* **2000**, *374*, 303. (b) Tachi, S. *J. Vac. Sci. Technol.* **2003**, *A21*, S131.

(4) (a) Hiraoka, K.; Takao, K.; Iino, T.; Nakagawa, F.; Suyama, H.; Mizuno, T.; Yamabe, S. *J. Phys. Chem. A* **2002**, *106*, 603. (b) Hiraoka, K.; Fujita, K.; Ishida, M.; Okada, K.; Hizumi, A.; Wada, A.; Yamabe, S.; Tsuchida, N. *J. Phys. Chem. A* **2005**, *109*, 1049.

(5) Shiotani, M.; Kawazoe, H.; Sohma, J. *Chem. Phys. Lett.* **1984**, *111*, 254.

(6) Hasegawa, A.; Shiotani, M.; Hama, Y. *J. Phys. Chem.* **1994**, *98*, 1834.

(7) Itagaki, Y.; Shiotani, M.; Hasegawa, A.; Kawazoe, H. *Bull. Chem. Soc. Jpn.* **1998**, *71*, 2547.

(8) Shiotani, M.; Kawazoe, H.; Sohma, J. *J. Phys. Chem.* **1984**, *88*, 2220.

(9) Ohta, K.; Shiotani, M.; Sohma, J. *Chem. Phys. Lett.* **1987**, *140*, 148.

(10) (a) Shiotani, M.; Persson, P.; Lunell, S.; Lund, A.; Williams, F. *J. Phys. Chem. A* **2006**, *110*, 6307.(b) Shiotani, M.; Lund, A.; Lunell, S.; Williams, F. *J. Phys. Chem. A* **2007**, *111*, 321.

(11) Karna, S. P.; Grein, F.; Engels, B.; Peyerimhoff, S. D. *Int. J. Quantum Chem.* **1989**, 255.

(12) Feller, D. *J. Chem. Phys.* **1990**, *93*, 579.

(13) Li, W.-Z.; Huang, M.-B. *J. Mol. Struct. (THEOCHEM)* **2003**, *636*, 71.

(14) Chang, C. H.; Andreassen, A. L.; Hbaiter, S. H. S. *J. Org. Chem.* **1971**, *36*, 920.

(15) Aston, J. G.; Sasz, G.; Woolley, H. W.; Brickwedde, F. G. *J. Chem. Phys.* **1946**, *14*, 67.

(16) Brundle, C. R.; Robin, M. B. *J. Am. Chem. Soc.* **1970**, *92*, 5550.

(17) Hohenberg, P.; Kohn, W. *Phys. Rev. B* **1964**, *136*, 785.

(18) Kohn, W.; Sham, L. J. *Phys. Rev. A* **1965**, *140*, 1133.

(19) Becke, A. D. *J. Chem. Phys.* **1993**, *98*, 5648.

(20) Lee, C.; Yang, W.; Parr, R. G. *Phys. Rev. B* **1988**, *37*, 785.

(21) Møller, C.; Plesset, M. S. *Phys. Rev.* **1934**, *46*, 618.

(22) Pople, J. A.; Binkley, J. S.; Seeger, R. *Int. J. Quantum Chem. Symp.* **1976**, *10*, 1.

(23) Roos, B. O.; Taylor, P. R.; Siegban, P. E. M. *Chem. Phys.* **1980**, *48*, 157.

(24) Roos, B. O. *Int. J. Quantum Chem.* **1980**, *S14*, 175.

(25) Andersson, K.; Malmqvist, P.-Å.; Roos, B. O. *J. Chem. Phys.* **1992**, *96*, 1218.

(26) Andersson, K. *Theor. Chim. Acta* **1995**, *91*, 31.

(27) Finley, J.; Malmqvist, P.-Å.; Roos, B. O.; Serrano-Andrés, L. *Chem. Phys. Lett.* **1998**, *288*, 299.

(28) Wurrey, C. J.; Bucy, W. E.; Durig, J. R. *J. Chem. Phys.* **1977**, *67*, 2765.

(29) (a) Shiotani, M. *Magn. Reson. Rev.* **1987**, *12*, 333. (b) Lindgren, M.; Shiotani, M. In *Radical Ionic Systems: Properties in Condensed Phases*; Lund, A., Shiotani, M., Eds.; Kluwer Academic Publishers: Dordrecht, The Netherlands, 1991; p 125. (c) Shiotani, M.; Lund, A. In *Radical Ionic Systems: Properties in Condensed Phases*; Lund, A., Shiotani, M., Eds.; Kluwer Academic Publishers: Dordrecht, The Netherlands, 1991; p 151. (d) Shiotani, M.; Yoshida, H. In *CRC Handbook of Radiation Chemistry*; Tabata, Y., Ed.; CRC Press: Boca Raton, FL, 1991; pp 440−467.

(30) Woon, D. E.; Ding, T. H., Jr. *J. Chem. Phys.* **1993**, *98*, 1358.

(31) Davidsion, E. R. *Chem. Phys. Lett.* **1996**, *220*, 514.

(32) Frisch, M. J.; Trucks, G. W.; Schlegel, H. B.; Scuseria, G. E.; Robb, M. A.; Cheeseman, J. R.; Montgomery, J. A., Jr.; Vreven, T.; Kudin, K. N.; Burant, J. C.; Millam, J. M.; Iyengar, S. S.; Tomasi, J.; Barone, V.; Mennucci, B.; Cossi, M.; Scalmani, G.; Rega, N.; Petersson, G. A.; Nakatsuji, H.; Hada, M.; Ehara, M.; Toyota, K.; Fukuda, R.; Hasegawa, J.; Ishida, M.; Nakajima, T.; Honda, Y.; Kitao, O.; Nakai, H.; Klene, M.; Li, X.; Knox, J. E.; Hratchian, H. P.; Cross, J. B.; Adamo, C.; Jaramillo, J.; Gomperts, R.; Stratmann, R. E.; Yazyev, O.; Austin, A. J.; Cammi, R.; Pomelli, C.; Ochterski, J. W.; Ayala, P. Y.; Morokuma, K.; Voth, G. A.; Salvador, P.; Dannenberg, J. J.; Zakrzewski, V. G.; Dapprich, S.; Daniels, A. D.; Strain, M. C.; Farkas, O.; Malick, D. K.; Rabuck, A. D.; Raghavachari, K.; Foresman, J. B.; Ortiz, J. V.; Cui, Q.; Baboul, A. G.; Clifford, S.; Cioslowski, J.; Stefanov, B. B.; Liu, G.; Liashenko, A.; Piskorz, P.; Komaromi, I.; Martin, R. L.; Fox, D. J.; Keith, T.; Al-Laham, M. A.; Peng, C. Y.; Nanayakkara, A.; Challacombe, M.; Gill, P. M. W.; Johnson,

B.; Chen, W.; Wong, M. W.; Gonzalez, C.; Pople, J. A. *Gaussian 03*, revision B.02; Gaussian Inc.: Pittsburgh, PA, 2003.

(33) Karlström, G.; Lindh, R.; Malmqvist, P.-Å.; Roos, B. O.; Ryde, U.; Veryazov, V.; Widmark, P.-O.; Cossi, M.; Schimmelpfennig, B.; Neogrady, P.; Seijo, L. *Comput. Mater. Sci.* **2003**, *28*, 222.

(34) Veryazov, V.; Widmark, P. O.; Serrano-Andres, L.; Lindh, R.; Roos, B. O. *Int. J. Quantum Chem.* **2004**, *100*, 626.

(35) Roos, B. O.; Lindh, R.; Malmqvist, P.-Å.; Veryazov, V.; Widmark, P.-O. *J. Phys. Chem. A* **2004**, *108*, 2851.

(36) Widmark, P.-O.; Malmqvist, P.-Å.; Roos, B. O. *Theor. Chim. Acta* **1990**, *77*, 291.

(37) Widmark, P.-O.; Persson, B. J.; Roos, B. O. *Theor. Chim. Acta* **1991**, *79*, 419.

(38) Karpfen, A. *J. Phys. Chem. A* **1999**, *103*, 2821.

(39) Dixon, D. A. *J. Phys. Chem.* **1986**, *90*, 2038.

(40) Choudhury, T.; Scheiner, S. *J. Mol. Struct. (THEOCHEM)* **1984**, *109*, 373.

(41) Foley, M. S. C.; Braden, D. A.; Hudson, B. S.; Zgierski, M. Z. *J. Phys. Chem. A* **1997**, *101*, 1455.

(42) http://csep10.phys.utk.edu/astr162/lect/light/spectrum.html.